JGR Atmospheres

RESEARCH ARTICLE
10.1029/2019JD032283

Erythemal Radiation, Column Ozone, and the North American Monsoon

M. R. Schoeberl[1], L. Pfister[2], T. Wang[3], J. Kummer[1], A. E. Dessler[4], and W. Yu[4]

[1]Science and Technology Corporation, Columbia, MD, USA, [2]NASA Ames Research Center, Moffett Field, CA, USA, [3]Jet Propulsion Laboratory/California Institute of Technology, Pasadena, CA, USA, [4]Department of Atmospheric Sciences, Texas A&M University, College Station, TX, USA

Key Points:
- We find a positive correlation between summer lower stratospheric water vapor anomalies and erythemal radiation over the southwest United States
- This correlation is the result of a monsoonal convection lifting the tropopause, reducing the ozone column, and increasing the surface UV
- We find no apparent evidence of substantial chemical ozone depletion in the lower stratosphere due to convective injection of water vapor

Correspondence to:
M. R. Schoeberl,
mark.schoeberl@mac.com

Citation:
Schoeberl, M. R., Pfister, L., Wang, T., Kummer, J., Dessler, A. E., & Yu, W. (2020). Erythemal radiation, column ozone, and the North American monsoon. *Journal of Geophysical Research: Atmospheres*, *125*, e2019JD032283. https://doi.org/10.1029/2019JD032283

Received 28 DEC 2019
Accepted 26 MAY 2020
Accepted article online 29 MAY 2020

Author Contributions:
Conceptualization: M. R. Schoeberl
Data curation: T. Wang, W. Yu
Formal analysis: M. R. Schoeberl
Investigation: M. R. Schoeberl
Methodology: M. R. Schoeberl
Resources: A. E. Dessler
Software: M. R. Schoeberl, W. Yu
Validation: M. R. Schoeberl
Writing - original draft: M. R. Schoeberl
Writing – review & editing: M. R. Schoeberl, T. Wang, A. E. Dessler

Abstract Recently, Anderson et al. (2012, https://doi.org/10.1126/science.1222978, 2017, https://doi.org/10.1073/pnas.1619318114) and Anderson and Clapp (2018, https://doi.org/10.1039/C7CP08331A) proposed that summertime convectively injected water vapor over North America could lead to stratospheric ozone depletion through halogenic catalytic reactions. Such ozone loss would reduce the ozone column and increase erythemal daily dose (EDD). Using 10 years of observations over the North American monsoon region from the Aura Ozone Monitoring Instrument, we find that the column ozone and EDD has a ~0.8–0.9 spatial correlation with lower stratospheric water vapor measured by the Aura Microwave Limb Sounder. We show that this correlation appears to be due to the elevation of the monsoonal tropopause and associated monsoonal convection. The increase in tropopause altitude reduces the ozone column and increases EDD. We see no apparent evidence of substantial heterogeneous chemical ozone loss in lower stratospheric ozone coincident with the stratospheric monsoonal water vapor enhancement.

Plain Language Summary Anomalously high surface ultraviolet (UV) radiation is present over southwest United States during the July–August North American monsoon. This elevated radiation results from the lifting of the tropopause and subsequent reduction of the ozone column. Simultaneously, water vapor in the upper troposphere and lower stratosphere (UTLS) increases as a result of the monsoon convection. Thus, summer monsoon increases in UV radiation and the erythemal daily dosage are correlated with enhanced UTLS water vapor, but this correlation does not appear to be a signal of unusual stratospheric chemical ozone loss.

1. Introduction

Anderson et al. (2012) suggested that the convective moistening of the summer North American monsoon (NAM) lower stratosphere might lead to catalytic ozone loss. The basic idea is that increased water vapor from summertime monsoon convection near the cold tropopause would increase the heterogeneous chlorine reaction probability (Shi et al., 2001) as well as the surface area of ambient sulfuric acid aerosols (Drdla & Müller, 2010 producing chlorine radicals that would catalytically destroy ozone. Indeed, aircraft measurements by Thornton et al. (2007) showed elevated chlorine radical concentration over the continental United States in early April 1998, coincident with high aerosol and water vapor amounts and gravity wave-induced cold temperatures. Thus, in a process somewhat similar to that observed by Thornton et al. (2007), deep convection, penetrating into the stratosphere, could produce summertime ozone loss. This loss would occur during the season of maximum surface ultraviolet (UV) radiation, and the consequential increase in surface UV radiation and erythemal dosage might lead to widespread health effects (Anderson & Clapp, 2018; WHO, 2006; hereafter AC).

The Anderson et al. (2012) hypothesis is controversial, and the notion that significant summer ozone loss might be occurring was criticized by Schwartz et al. (2013). They noted that while Aura Microwave Limb Sounder (MLS) measurements show convective plumes of water vapor over the NAM, as has been observed by aircraft during the Studies of Emissions and Atmospheric Composition, Clouds and Climate Coupling by Regional Surveys (SEAC^{4}RS) mission and other aircraft missions (Hanisco et al., 2006; Herman et al., 2017; Smith et al., 2017; Thornton et al., 2007), the concentration Cl_y required for halogen catalyzed ozone loss was likely too low to cause an ozone losses of a sufficient magnitude to pose a human health risk. Schwartz et al. (2013) also noted that in the midlatitude lower stratospheric temperatures are generally too warm to activate aerosols as heterogenous reaction surfaces.

In another study, Homeyer et al. (2014) analyzed the transport of trace gases during the spring 2012 NASA Deep Convective Clouds and Chemistry (DC3) experiment. They found that deep convection processes facilitated a double tropopause condition and that deep convection injected ice into an air mass compositionally quite different from the lower stratosphere—an air mass with low concentration of inorganic chlorine based on correlations with ozone and CO.

Anderson et al. (2017) addressed some of the issues raised by Schwartz et al. (2013). Anderson et al. (2017) pointed to the observed correlation between ozone and HCl, which suggested that there might be sufficient HCl in the lower stratosphere for the heterogeneous chemical ozone loss at the highest convective injection altitudes. They also noted that aircraft temperature observations made during SEAC^{4}RS were ~1–5 K colder than GPS radio occultation temperatures used in reanalysis systems. The SEAC^{4}RS observed temperatures are at the upper end of the range required for aerosol activation when convectively enhanced water vapor is present.

Recently, Robrecht et al. (2019) has revisited the SEAC^{4}RS data and used the CLAMS model to explore the possibility of chemical ozone loss following the convective injection of water vapor into the lower stratosphere. With a series of model experiments, they found that the injected water vapor amount had to exceed 10 ppmv, and there had to be sufficient aerosol nuclei and high amounts of reservoir chlorine (~1 ppbv of Cl_y) to produce ~60% ozone loss. They found that under normal summer midlatitude conditions, Cl_y is believed to be ~0.15 ppbv (based on observed correlation with CH_4) and with a 20 ppmv injection of water, Robrecht et al. (2019) computed an ozone loss of only ~9%. According to MLS observations compiled by Schwartz et al. (2013) convectively injected water levels exceeding 20 ppmv are rarely observed at 16 km (~100 hPa) and higher altitudes.

Is ozone depletion occurring subsequent to convective injection of water vapor? If so, how much depletion occurs? One of the many goals of the NASA Dynamics and Chemistry of the Summer Stratosphere (DCOTSS) aircraft mission (https://espo.nasa.gov/dcotss; also see *Science*, 364, pp. 322–325) is to explore the chemical and dynamical processes within the NAM. In addition to in situ aircraft measurements, an obvious study that might support or refute halogenic chemical loss is to examine the MLS water vapor and ozone measurements along with the Ozone Monitoring Instrument (OMI) estimate of erythemal daily dose (EDD) and column ozone measurements. Under the high chlorine scenario, Anderson et al. (2017) and AC estimated that there could be as much as a 7% ozone column reduction due to chemical ozone loss. EDD is highly anticorrelated with column ozone (−0.93); more specifically δ [EDD] ~ −0.06 δ [Column O_3] where column O_3 is in DU and EDD is in kJ/m^2. Over the United States, the July–August average ozone column is ~276 DU. A 7% decrease in column O_3 is equivalent to ~20 DU; this would produce an EDD increase of 1.2 kJ/m^2. Over North America, EDD varies from 3–6 kJ/m^2 (see Figure 4a below) so a 1.2 kJ/m^2 increase in EDD would be a health concern.

Extratropical monsoonal convection can produce large scale plumes of cirrus extending several kilometers above the anvil (Homeyer et al., 2017). Under high Cl_y scenarios, ozone loss in the presence of enhanced water vapor would take place in 5–10 days (Robrecht et al., 2019, Figure 11), and both the ozone loss and water vapor plume would spread over the lower stratospheric monsoon region. Given that the normal lifetime of ozone in the UTLS is weeks to months (Brasseur & Solomon, 2016), the signature of ozone loss should be quite evident since the lifetime of parcels trapped with the monsoon can be on the order of weeks (Clapp et al., 2019). An ozone loss of this magnitude should clearly be detectable in changes in OMI column ozone and EDD and evident in MLS stratospheric ozone profiles. Thus, we hypothesize that if significant heterogeneous chemistry were occurring, a chemical loss signal would likely be detectable in the lower stratospheric ozone profiles, the ozone column, and/or EDD during the NAM. The depletion of lower stratospheric ozone would be correlated with enhanced water vapor and the presence of convection. This paper explores the connection between the NAM water vapor, column and profile ozone, and EDD using MLS and OMI observational data sets along with convective height estimates produced by L. Pfister.

2. Observational Data Sets

For the dynamical fields, we use the European Centre for Medium-Range Weather Forecasts (ECMWF)-interim (ERAi) reanalysis meteorological analysis (Dee et al., 2011) averaged into 2.5° × 2.5° latitude-longitude bins. Trace gas and convective height data sets are described below.

2.1. MLS and OMI Trace Gas Data

We use MLS V4.2 measurements of ozone, CO, and water vapor (see Livesey et al., 2017 for product descriptions and validation). MLS retrievals have a vertical resolution of ~3 km around the tropopause. In addition to the MLS measurements, we use the measurements of column ozone and EDD produced from Aura's OMI (Levelt et al., 2006; Tanskanen et al., 2007). OMI measures surface spectral irradiance at 305, 310, 324, and 380 nm from which the amount of UV radiation reaching the surface of the Earth is computed after correcting for attenuation and absorption of the direct solar beam. The OMI algorithm computes the amount of Rayleigh scattering, ozone absorption, multiple scattering by clouds, scattering and absorption by aerosols, and reflection from the surface. Using the estimated surface UVA and UVB radiation (UVA, 320–400 nm; UVB, 290–320 nm), Caucasian skin-type damage associated with sunburn (EDD) is computed. The original OMI erythemal algorithm has been recently updated to correct for boundary layer aerosols (Arola et al., 2009). Additional validation studies comparing the OMI product with surface UV measurements made by U.S. Department of Agriculture Ultraviolet Monitoring and Research Program show that the OMI correlation to surface UV measurements is about 0.9, and that OMI is high biased by ~7% (Zhang et al., 2019; Zhou et al., 2019).

2.2. Convective Heights

In order to understand the pattern of convection during the monsoon, we use the global convective height product produced by L. Pfister (see Schoeberl et al., 2019; Ueyama et al., 2014). The Pfister convective height product is available every 3 hr on a 0.25° × 0.25° grid. To determine the convective region, the algorithm uses a rain rate threshold from the Global Precipitation Mission 3B42 data set (Huffman et al., 2007). The rain rate thresholds vary in latitude and longitude and are derived by matching rain rate with the statistics of the incidence of CloudSat deep convection (Sassen & Wang, 2008). Convective altitudes and potential temperatures are calculated by matching infrared (IR) brightness temperatures in the convective regions (using the coldest brightness temperatures within each 0.25° × 0.25° degree grid box) with temperature profiles from the National Oceanic and Atmospheric Administration (NOAA) Global Forecast System analyses. Brightness temperatures are available from the NASA Goddard Earth Sciences Data and Information Services Center (GES DISC) as the GPM_MERGIR: National Center for Environmental Prediction/Climate Prediction Center L3 (NCEP/CPC L3) data set.

Comparisons with Cloud-Aerosol Lidar with Orthogonal Polarization (CALIOP) measurements are used to correct the convective top biases (Minnis et al., 2008; Sherwood et al., 2004). The result is a 3-hourly convective cloud top product whose statistics match combined CloudSat and CALIOP measurements. For locations where the brightness temperatures are colder than the level of neutral buoyancy (near the tropopause) (LNB), a simple mixing algorithm is used to create a temperature profile above the LNB. This temperature profile is then matched with the brightness temperature to calculate the altitude and potential temperature.

Next Generation Weather Radar (NEXRAD) convective cloud tops over the United States are higher than the Pfister convective cloud tops in that region (for details on the NEXRAD product, see Cooney et al. (2018)). Although the Pfister product includes adjustments derived from comparisons of IR based cloud tops and CALIOP measurements, regional biases remain over North America for three reasons. First, the tops of the deepest convection extend far enough into the stratosphere that they may actually be warmer than lower cloud tops. In other words, the temperature profile matching on which IR cloud top altitude estimation method depends can fail for very deep clouds (Homeyer, 2014). Second, the geostationary IR methods are based on 4 km pixels, and a significant number of the deepest overshooting tops are smaller than this in size. Third, the NEXRAD temporal sampling is nearly continuous, whereas the geostationary IR data is, at best, a half-hourly snapshot. NEXRAD can capture brief convective penetrations that reach high altitudes, while the IR methods will not detect these overshoots since the ice crystals evaporate rapidly in the dry stratosphere. Figures 1a and 1b shows a 12 year, June-July-August, comparison of the normalized fraction of convective tops exceeding 16 km (~100 hPa) for both NEXRAD and Pfister convection over the continental United States (Gulf region is excluded). Both plots show the fractional occurrences within 1° × 1° grid box normalized over the area (25–49°N, 65–100°W). The correlation between the two products is about 0.78. The NEXRAD and Pfister spatial distribution of convective systems reaching 100 hPa generally agree except in regions not well covered by NEXRAD (e.g., mountainous regions). Methodological differences in labeling convection likely explain the local Pfister convection maximum in the southeast United States, which is not

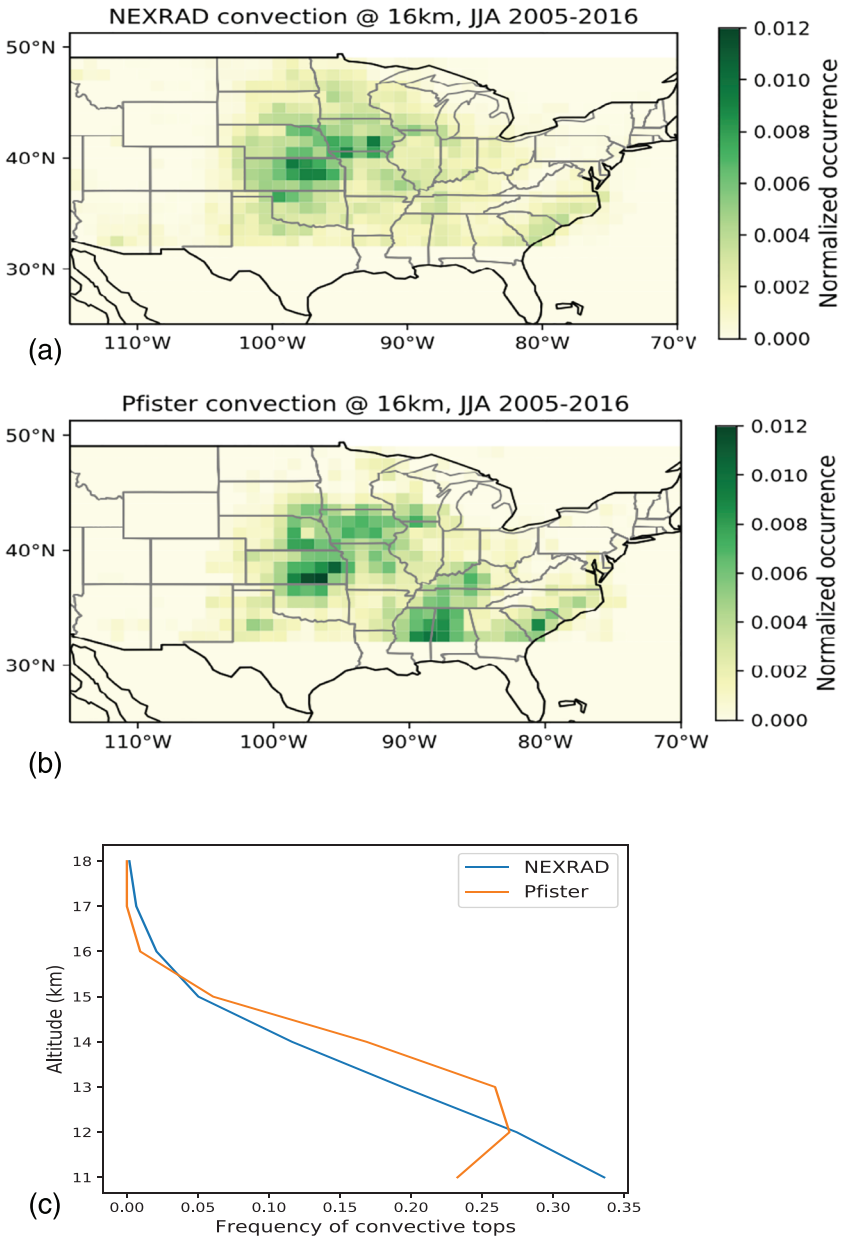

Figure 1. Comparison between NEXRAD convection (a) and the Pfister convection (b). The statistics are the normalized fraction of convective events with tops above 16 km (~100 hPa) for June-July-August 2005–2016; see text for details. The total frequency summed over the area equals 1 for both maps. (c) Frequency of convective tops versus altitude over the continental United States comparing Pfister and NEXRAD; each level is normalized to 1.

evident in NEXRAD. In particular, the Pfister scheme uses a similar rain rate threshold to label convection for all North American land-based convection, which may not fully account for differences in how convection produces rainfall in the different regions. Also, convection with slower ascent rates will tend to have smaller particles near the top, which NEXRAD (unlike the IR methods) will not be sensitive to. Figure 1c shows the frequency of convective tops versus altitude. The two products compare well although NEXRAD reports slightly larger frequency at the highest altitudes, whereas Pfister convection shows a higher frequency at lower altitudes. Despite some of the shortfalls in the Pfister product, the overall picture of monsoon convection over the continental United States is quite similar to NEXRAD. The distinct advantage of Pfister convection over NEXRAD is that it extends the coverage to Mexican monsoon region.

The average convective height statistics shown in Figures 5–7 below are computed by ignoring all convective heights below 10 km (~240 hPa) and averaging the July–August convective heights in each cell. Ten years of July–August convective and trace gas data is analyzed for the period 2006–2015. This averaging should reduce the interannual variability associated with the monsoon (Clapp et al., 2019) and allow the emergence of a mean signal if one exists.

3. The Monsoons

Basic monsoon dynamics are summarized in Zhisheng et al. (2015). The boreal monsoons typically form in late June, reach peak amplitude during July and August, then taper off in September. The monsoon circulations are basically giant sea breeze systems with the summertime heated land producing wide-scale upward motion. This heating is especially intense at higher elevations so that the monsoons preferentially form over the Himalayan and Colorado plateaus. The heating and upward motion produces convergence at low levels that brings in moisture from nearby oceans. The combination of heating and moisture convergence produces local regions of high convective available potential energy (CAPE) and subsequent widespread convection reinforces the monsoon circulation. The horizontal scale of the monsoon system exceeds the Rossby radius of deformation and, as a result, a cyclonic pressure system forms in the convergence zone at the base of the monsoon. With upward motion at the core of the monsoon, the divergent outflow at higher altitudes produces an anticyclonic circulation and the upward motion lifts the tropopause. The two major boreal monsoons are the extensive Asian monsoon (AM) that forms over India and adjacent regions, and the smaller NAM that forms over the southern United States and northern Mexico.

To illustrate the effect of the monsoon on ozone and EDD, Figure 2 shows 2006–2015 July–August average column ozone, EDD as well as MLS measured traces gases, CO, ozone, and water vapor in the upper troposphere and lower stratosphere (UTLS) at 100 hPa (~16 km). Both the AM and NAM show lower column ozone and elevated EDD compared to other longitudes. The monsoon's high-altitude anticyclonic circulation tends to isolate the trace gases brought into the region by convection (e.g., Pan et al., 2016; Park et al., 2007; Santee et al., 2017). This is clearly seen in both the CO (Figure 2e) and H_2O fields (Figure 2d) over the AM. The NAM H_2O and CO anomalies are weaker because (1) the weaker isolating upper-level circulation compared to the AM, and (2) in the case of CO, there is more surface pollution underneath the AM to create the CO anomaly compared to the NAM (Bergman et al., 2013; Pan et al., 2016). Both monsoons also show an ozone anomaly, but the 10 year averaging tends to merge the anomaly with the tropical ozone fields, so the anomalies appear as a northward extension of the tropical ozone regions (Figure 2c).

Figure 3 shows the July–August zonal mean trace gas fields shown in Figure 2 to provide an overview of the upper troposphere and stratospheric vertical structure. The zonal mean tropopause descends rapidly from the tropics to the higher latitudes. Below the zonal mean tropopause, tropical water vapor and CO fields bulge upward as a result of convection.

3.1. The NAM

The NAM circulation is not as strong as the AM because of less surface heating on the Colorado Plateau which has a lower elevation than the Himalayan Plateau. In addition, the Gulf of California and Gulf of Mexico moisture sources are more intermittent than that of the Indian Ocean. The most intense NAM convection is found in the southwest United States and northern Mexico (as we shall show below, Figure 4c) (Adams & Comrie, 1997). The center of the monsoon anticyclone is located over northern Mexico at 146 hPa and moves northward and weakens with altitude. At 100 hPa, the anticyclone is centered over northern New Mexico with the circulation extending over most of the western United States and Mexico. At 82 hPa the anticyclone is centered over eastern Wyoming.

As an initial test of the possible column ozone changes associated with convectively injected water, we correlated EDD and water vapor at 100 and 82 hPa (the lower stratosphere) over the NAM July–August period using 10 years of July–August observations; at 100 hPa the correlation is 0.72, and at 82 hPa the correlation is 0.77 (Table 1). This correlation is consistent with the Anderson hypothesis—higher water vapor concentration activates aerosols and produces chemical ozone loss thereby increasing the dosage. However, as seen in Table 1, at altitudes below 100 hPa, the correlation is even higher. For example, at 121 hPa the correlation is 0.85. Generally, HCl concentrations are much lower at 121 hPa compared to 82 hPa based on the observed

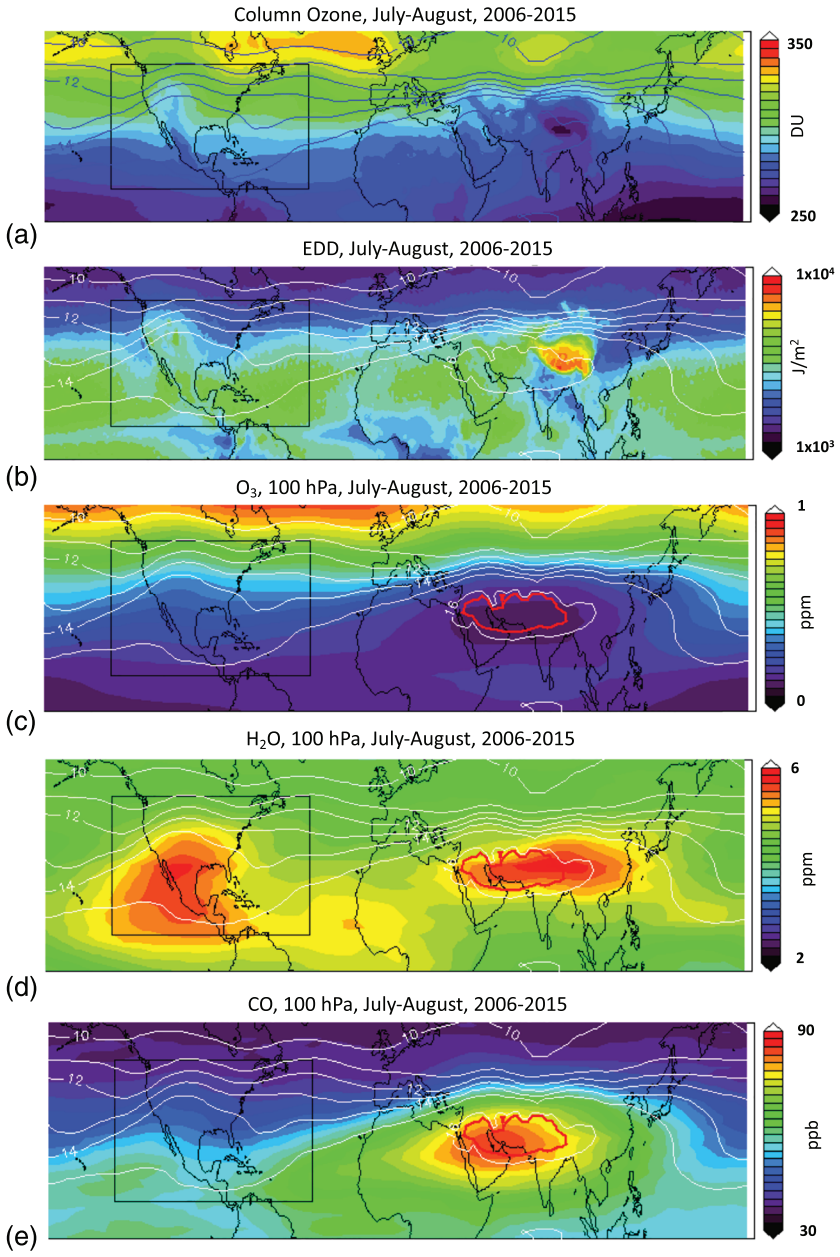

Figure 2. Ten-year average (2006–2015) of (a) column ozone, (b) EDD, MLS trace gases (c) O_3, (d) H_2O, and (e) CO at 100 hPa. The white contours show the log-pressure height of the tropopause, and the red contour shows where ERAi tropopause intersects the 100 hPa level in the AM region. The NAM region analyzed below is outlined with the box.

decrease in HCl abundance with altitude (Froidevaux et al., 2015). Therefore, the high correlation between EDD and water vapor is more likely due to processes other than heterogeneous chemical loss. Below we examine dynamical factors that could explain the water vapor-EDD correlation by examining the NAM trace gas fields and circulation at four upper tropospheric/lower stratospheric MLS levels, 146 hPa (~13.4 km), 121 hPa (~14.7), 100 hPa (~16.1 km), and 82 hPa (~17.4 km).

3.2. The NAM Column Ozone, EDD, Convection and Trace Gases

The correlation between the NAM EDD and column ozone is −0.89, that is, higher column ozone, less EDD. Column ozone is also highly correlated with tropopause height (Staehelin et al., 2001; Steinbrecht et al., 1998). Given a constant ozone column, geographic elevation will also influence EDD. To illustrate these

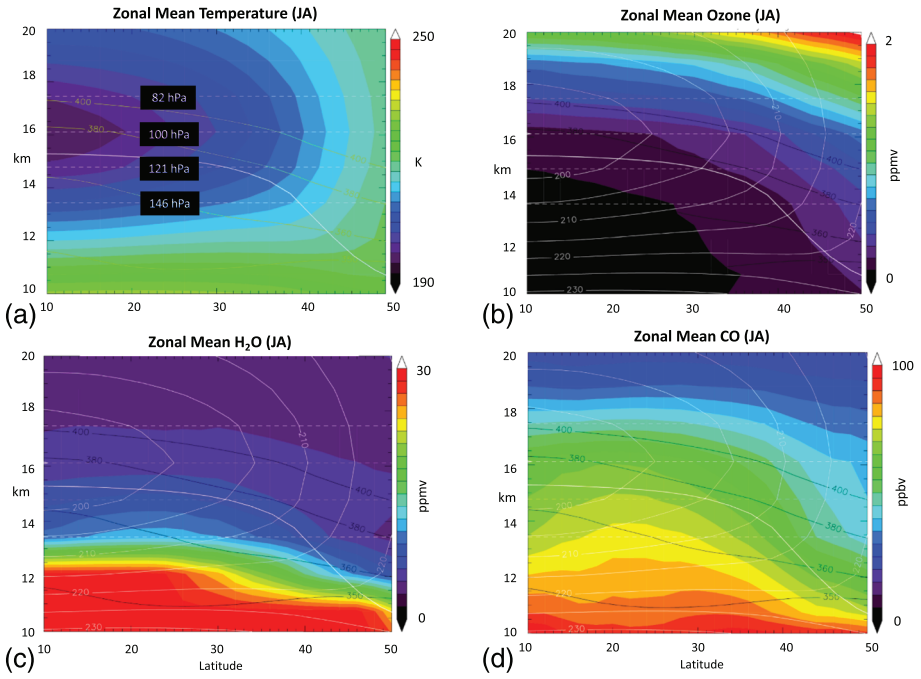

Figure 3. Ten-year average zonal mean July–August trace gas distribution versus pressure-altitude. (a) Zonal mean temperature. (b) Ozone mixing ratio; white contours are temperature from (a). (c) Water vapor mixing ratio. (d) CO mixing ratio. Dashed line shows the MLS pressure surfaces; although CO is reported on every other surface shown. Thicker white line is the zonal mean tropopause. Black contours are potential temperature surfaces.

factors, Figure 4 shows EDD, column ozone, elevation, and cloud fraction for the NAM region. Tropopause height contours are overlaid on the maps. Figure 4a shows the increase in EDD over the southwestern United States compared to surrounding regions at the same latitude. (The hot spot over Mexico City is due to high levels of aerosol scattering.) Column ozone shows the same distribution (Figure 4b), and both are coincident with elevated tropopause height as well as increased surface elevation (Figure 4c). The cloud fraction plot (Figure 4d) shows that there is a slight increase in clouds over the Rocky Mountains, but the increase in clouds is not large. Clouds slightly reduce EDD. Note that there is also more variability in the EDD field than the tropopause height or the column ozone. This variability is due to changes in EDD with elevation as discussed below.

Table 2 summarizes the spatial correlations between tropopause height variations, elevation, EDD, column ozone, and water vapor at the four pressure levels. In computing the correlation with topography, we consider only elevations greater than 100 m to screen out oceanic data. Table 2 shows that the anticorrelation between column ozone and elevation is not large compared to the anticorrelation between variations in tropopause height variations and column ozone (Staehelin et al., 2001). Not surprisingly, the magnitude of the correlation between tropopause height variations and EDD is similar to those with column ozone, but the correlation is not exactly the same because EDD also includes the effect of UV Rayleigh and aerosol scattering which changes with elevation and slightly reduces the correlation of EDD with tropopause height.

We perform a linear fit to the changes in column ozone or EDD relative to elevation or tropopause height ($DU = A + B\,z$ where z is the tropopause height or elevation height). The slope of the fits (B) are shown in Table 2. The slope calculated for the column ozone - tropopause height relationship is within the range reported by Steinbrecht et al. (1998). The change in EDD due to elevation is smaller than the change in EDD due to tropopause height. As noted above, variations in EDD are also sensitive to variations in Rayleigh and aerosol scattering. The change in elevation in the American Southwest is roughly of the same magnitude as the change in tropopause height over the monsoon region as we will show below (Figures 4 and 6), but based on the linear fits, the sensitivity of the column ozone to tropopause height is greater than the sensitivity of column ozone to elevation. The fits show that, as expected, EDD increases in the monsoon region are primarily due to changes in the tropopause height with a small enhancement correlated with elevation.

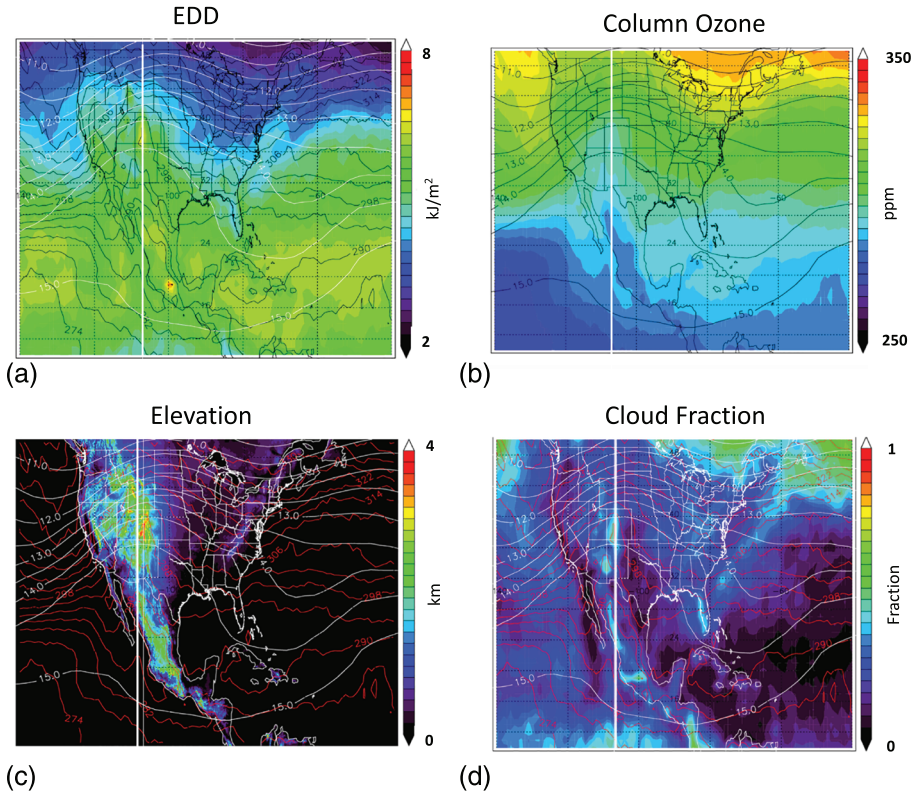

Figure 4. (a) EDD in kJ/m^2, black contours show column ozone in DU, white contours show tropopause height in km. (b) Column ozone and contours of tropopause height (black). (c) elevation in km, red contours are column ozone, white contours are tropopause height (km). (d) Cloud fraction with contours as in (c). Except for elevation, all quantities are 10 year averages (2006–2015) of July and August observations. Vertical white lines indicate 107°W for plots below.

Figures 5a–5c show 10-year average July–August maps of the 100 hPa (~16 km) H_2O and O_3. The extratropical 100 hPa level is entirely within the stratosphere at these latitudes. Wind vectors from ERAi reanalysis at this level show the weak anticyclonic circulation associated with the monsoon. These wind speeds are about 6–8 m/s over the monsoon which is centered over the southern United States. Figures 5c and 5d show Pfister average convective heights and frequency of convection penetrating the tropopause. The average height of convection (Figure 5c) shows that the highest convection is located throughout the American Southwest and northern Mexico - monsoon region. As mentioned above, the height average is computed using the number of convective events per grid cell above 10 km for the 10 year July–August periods on the 1/4° grid. The number of convective events that are higher than the local monthly mean tropopause average height over 10 years is shown in Figure 5d.

MLS ozone (Figure 5a) at 100 hPa roughly follows the tropopause height contours of the monsoon circulation. Low ozone is seen on the west side of the monsoon anticyclone, and higher ozone on the east side consistent with northward advection by the monsoon winds. Unlike ozone, H_2O shows local maximum covering northern Mexico and extending into the southwestern United States. Randel et al. (2015) found a similar distribution of water vapor in their 8-year climatology. The most obvious explanation for the water vapor distribution is that it is due to convective systems bringing up water from below followed by advection by the monsoon circulation (e.g., Dessler & Sherwood, 2004; Park et al., 2007; Wang et al., 2019). This process is even more evident at lower altitudes as we shall show below. Randel et al. (2012) found that the NAM monsoon water vapor was also the locus of elevated HDO, a marker of convection.

Consistent with the linkage between water vapor and convection, the higher convective events in western Mexico (Figure 4d) are roughly coincident with the large water vapor maximum over central Mexico. Since the monsoon winds are weak at these levels, water vapor from evaporating convective ice likely accumulates in the anticyclonic circulation, intensifying the anomaly. Randel et al. (2015) also noted the strong

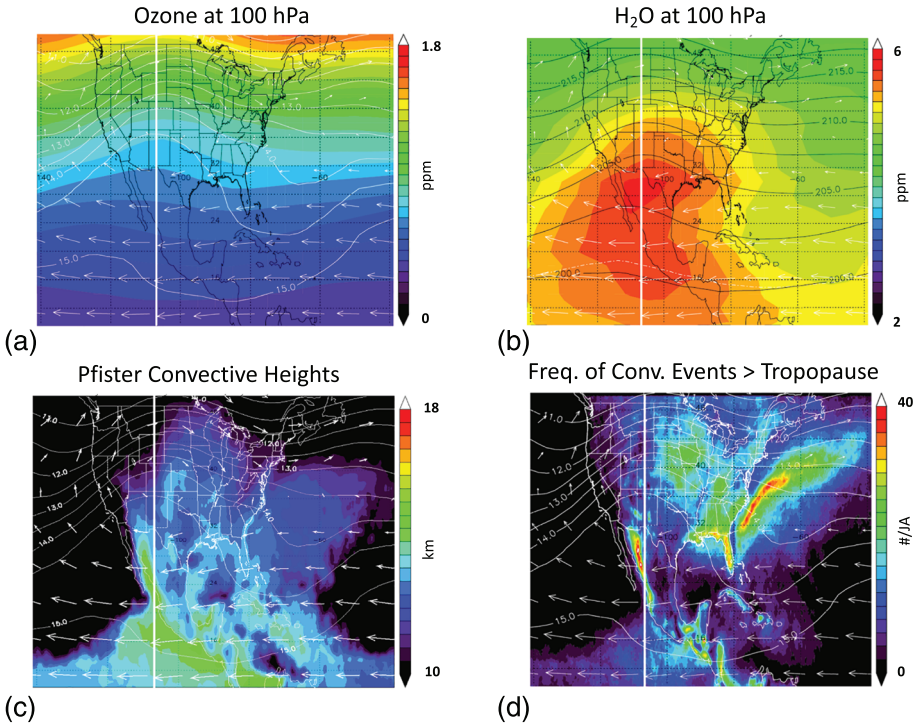

Figure 5. North American July–August monsoon fields averaged over 2005–2016. (a and b) As in Figures 2c and 2d but zoomed in over the NAM region. In Panels (a), (c), and (d), white contours are tropopause log-pressure height; in Panel (b), the black contours are temperature. White vectors indicate the wind direction and magnitude at 100 hPa. (c) The average height of convective events greater than 10 km. (d) The number of convective events that are higher than the local monthly mean tropopause using the Pfister convective heights. The vertical white line (107°W) indicates the location of the cross-section region shown in Figure 6 below.

connection between upper tropospheric water vapor and outgoing long wave radiation (OLR)—a measure of convective heights—as well as a slight offset between the highest frequency of convection and the water vapor field. Figure 5d also shows a region of slightly elevated frequency of stratospheric penetrating convection over the central Midwest as indicated in Figure 1, and as noted by Clapp et al. (2019) and Smith et al. (2017). The connection between convection and water vapor is also evident over the AM as seen in Figure 2 (Dessler & Sherwood, 2004; Pan et al., 2016; Park et al., 2007; Randel et al., 2012, 2015).

In order to further quantify the relationship between column ozone, water vapor, convection and tropopause height, we narrow our focus to the corridor shown as the N-S white line in Figures 4 and 5 at ~107°W. Figure 6 shows the change between this corridor and the nonmonsoon (nonconvective) region at the west edge of the Figures 4 and 5 maps (140°W). We difference the tropopause height, water vapor at 146 hPa, and column ozone between these two N-S transects. First, as expected, the ozone column difference tends to follow the tropopause height. The monsoon water vapor difference tends to follow the mean convective height, roughly parallel to the tropopause height. This explains the high anticorrelation between water vapor and column ozone seen in Table 1. In other words, because the NAM upper tropospheric water vapor anomaly correlates with the tropopause height, and since the column ozone anomaly anticorrelates with the tropopause height, water vapor and column ozone anticorrelate with each other. This anticorrelation is a result of the monsoon dynamics.

3.3. The UTLS Over the NAM

We next focus on a latitude cross section of temperature and trace gas fields at 107°W, and these figures can be compared to Figure 3, the zonal mean fields. Figure 7a shows the temperature at 107°W and the tropopause height at both 107°W (white line in Figure 4) and at 140°W (at the left edge of the map in Figure 5). This figure and Figure 6 illustrate how the extratropical tropopause is shifted up almost 2 km relative to the monsoon exterior locations. The figure also shows that the coldest region in the lower stratosphere

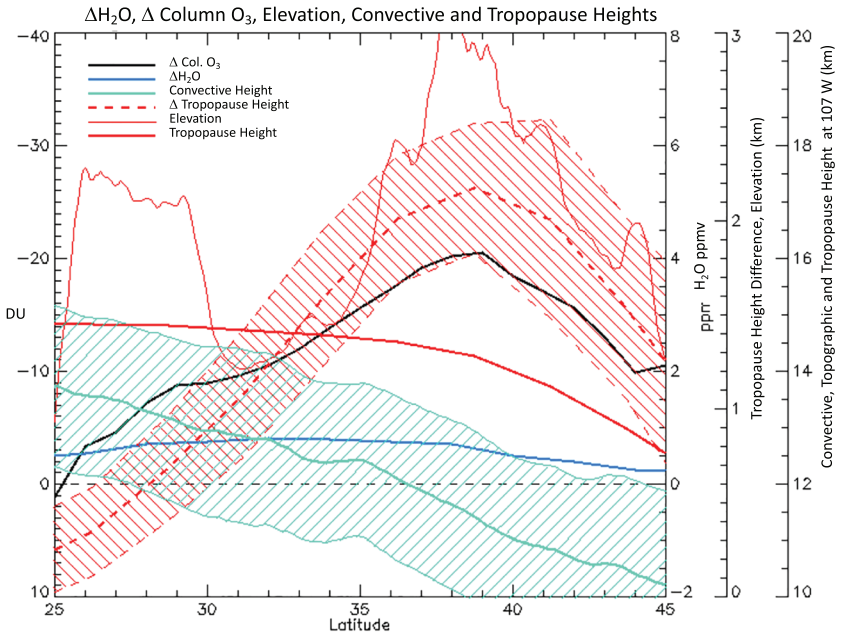

Figure 6. July–August 10 year average difference from 107°W (approximate monsoon longitude) to 140°W (107°W minus 140°W fields) for 146 hPa water (blue), column ozone (black), and tropopause height (red dashed). Also shown are the 107°W tropopause height (thick red line) with the year-to-year variability shown as red hatch region. Convective height and standard deviation envelope are shown as blue-green lines). The elevation at 107°W is a thin red line.

extends out from the tropics at these longitudes; this 14–17 km tropical extension would provide a preferential location for aerosol activation based on Figure 2 from Anderson et al. (2017), but because of its connection to the tropics, it is also a region with very low concentration of halogen reservoir gases (Froidevaux et al., 2015; Mahieu et al., 2008).

Figures 7b and 7c shows the difference in trace gas fields between 107°W and at 140°W—between the center of the monsoon and the edge. Figure 7b shows that the monsoon induced perturbation to ozone in the UTLS starts to decrease poleward of ~25°N. This is likely a direct result of adiabatic ascent as the flow moves northeastward over the elevated tropopause (Figure 5). From a Lagrangian perspective, lower mixing ratio ozone at 30°N and ~14 km moves northward upward to 16 km at 40°N. This should show up as an approximately 0.15 ppm decrease in ozone mixing ratio consistent with the results shown in Figure 7b. The water vapor field shown in Figure 7c also shows a clear increase over the whole lower stratosphere, but the largest increase is ~5 ppm up to the tropopause. Average convective heights at 107°W overlaid on the water vapor field provide more evidence that convective detrainment is increasing the water vapor field up to about 35°N. The overall picture of the monsoon shown in Figure 7 is consistent with Figure 6.

To investigate how the NAM signal varies in altitude around the 100 hPa level, Figure 8 shows maps of ozone and water vapor for the three other MLS levels 146 hPa (~13.4 km), 121 hPa (~14.7 km) and 82 hPa (~17.5 km). The 146 hPa surface is mostly in the upper troposphere over the monsoon region (see red line that marks the tropopause intersection). The 121 hPa surface crosses into the stratosphere at about ~25°N. These figures should be compared to the corresponding ones in Figure 5. The circulation (wind arrows) indicate that the monsoon high pressure system moves slightly north and east with altitude with easterlies strengthening at lower latitudes and westerlies weakening at higher latitudes. The ozone field becomes more zonal with altitude (Figures 8a–8c and 5a), and Figures 8d–8f and 5b show that the water vapor anomaly weakens with altitude (note the change in scaling between figures) presumably because convection rarely reaches the higher altitudes (Homeyer, 2014, also Figure 1c) along with less containment by the monsoon circulation.

AC simulations show that under optimal conditions following convective injection of 20 ppmv of water, the expected ozone loss between 13–18 km is 35–65%. Less ozone depletion would occur with lower

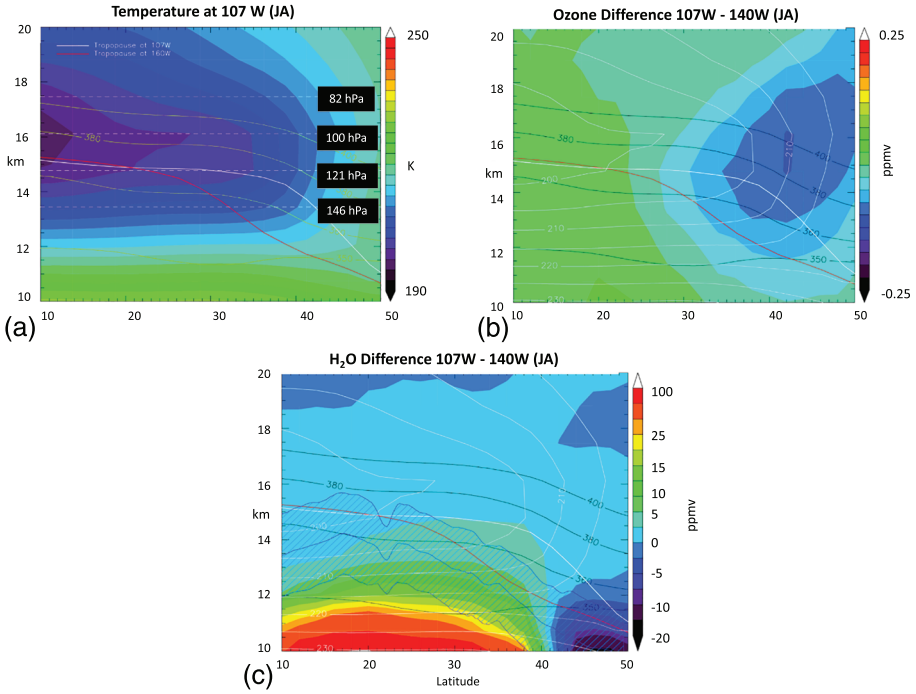

Figure 7. (a) Temperature and potential temperature at 107°W. Thick red line shows the tropopause altitude at 140°W (outside of the monsoon) and the white line at 90°W (inside the monsoon). Panels (b), (c), and (d) show differences between the NAM longitude (107°W) and nonmonsoon longitude (140°W) trace gases. (b) Ozone and (c) water vapor. Also shown in Panel (c) is the average convective height (thick blue line) and average convective height standard deviation (range of envelope).

concentration water vapor injections (Robrecht et al., 2019). An ozone depletion signature consistent with a water vapor mechanism is absent from the higher levels shown in Figure 8, particularly at 82 hPa (~17.5 km) despite the expectation that the 83 hPa and the 100 hPa region would best support the catalytic ozone loss as simulated by AC. In other words, the combination of water vapor and temperature observations shown in these figures do not appear to support a chemical mechanism as the leading cause for the observed ozone decrease in the monsoon region.

3.4. Column Effects of Convective Ozone Loss Compared to Tropopause Height Variations

Table 2 shows that changes in the observed ozone column can be approximated by δ[Column O_3 (DU)] ~ −9.2 δ [Tropopause height (km)] so that a 2 km increase in tropopause height as shown in Figure 6 translates into a change of ~18.4 DU. To further quantify changes in the ozone column through tropopause lifting verses changes due to chemical ozone loss, we have averaged the MLS ozone profiles from July and August, 2005–2013 from 30°N to 50°N and 110°W to 80°W (roughly the central United States) and imposed an ozone depletion "notch" as might be generated if there were rapid chlorine driven ozone loss from the excess convective water vapor. Homeyer et al. (2017) analyzed the satellite record for above-anvil extratropical cirrus plumes that would hydrate the stratosphere. They found that when plumes formed, they most frequently extended about 4 km above the tropopause. These plumes presumably form when breaking gravity waves mix moist tropospheric air upward (Qu et al., 2020). We use the simulations shown in AC and Robrecht et al. (2019) to define the upper and lower limit of a potential ozone depletion. We assume that water vapor is uniformly deposited from the top of the anvil to the top of the plume—an admittedly an upper bound case, a more realistic plume might hydrate a narrow layer with much less water vapor enhancement.

Table 1
Correlation Between Water Vapor and Column Ozone or EDD

Water vapor pressure level	Correlation with column O_3	Correlation with EDD
146 hPa	−0.76	0.7
121 hPa	−0.89	0.85
100 hPa	−0.82	0.72
82.5 hPa	−0.89	0.77

Table 2
Correlation Between Vertical Displacement and Column Ozone/EDD

Over the NAM region		Correlation with column O_3	Correlation with EDD	Slope of fit with column O_3 DU/km
Vertical displacement	Elevation	−0.27	0.32	-4.8 ± 0.5
	Tropopause	−0.9	0.85	-9.2 ± 0.127

Over the plume domain, ozone would decrease from ~1–2 × 10^{12} molecules to 0.4 × 10^{12} molecules for 1 ppb Cl_y (AC, Figure 14). For the lower Cl_y case (~0.15 ppbv) modeled by Robrecht et al. (2019), we impose uniform 9% ozone loss at each level noting that this amount of loss is likely an overestimate at lower altitudes since available chlorine increases with altitude. Figure 9a shows our MLS ozone profile modified by the two hypothetical ozone depletions for a 4.5 km plume extending from 12.5 to 17 km. Figure 9b shows the change in the ozone column as a function of different plume heights above the anvil. For a 4 km plume height, the maximum chemically induced change in ozone column is about 8.4 DU for the high chlorine case and ~1 DU using the low chlorine case. This can be compared to ~20 DU column ozone change due to the increase in the monsoon tropopause height as shown in Figure 9b. The ozone column reduction does not reach the 7% estimate from AC until the plume extends to ~18 km. This would be well above the probable height of convection (Figure 1c).

The bracket in Figure 9a indicates that for a plume depth ≥3 km, MLS should be able to detect the ozone loss coincident with the high water vapor. In the high chlorine case, the 100 hPa depletion would be ~0.25 ppm or about 60% of the ambient amount. Figures 5a and 8 do not show an ozone depletion of this magnitude coincident with the elevated water vapor. The evident lack of an ozone depletion in the MLS data was also noted by Schwartz et al. (2013).

Finally, it is possible that heterogeneous chemistry is taking place within a layer too shallow to be detected by MLS. This shallow layer could be formed either as a result of shearing deformation of the water vapor plume or as the result of a lower water vapor injection height. However, as the layer becomes shallower, the impact on column ozone is reduced as well. For a 1 km depth plume just above the tropopause, Figure 9b shows that the AC depletion produces ~1.5 DU change which corresponds to 0.5% decrease in

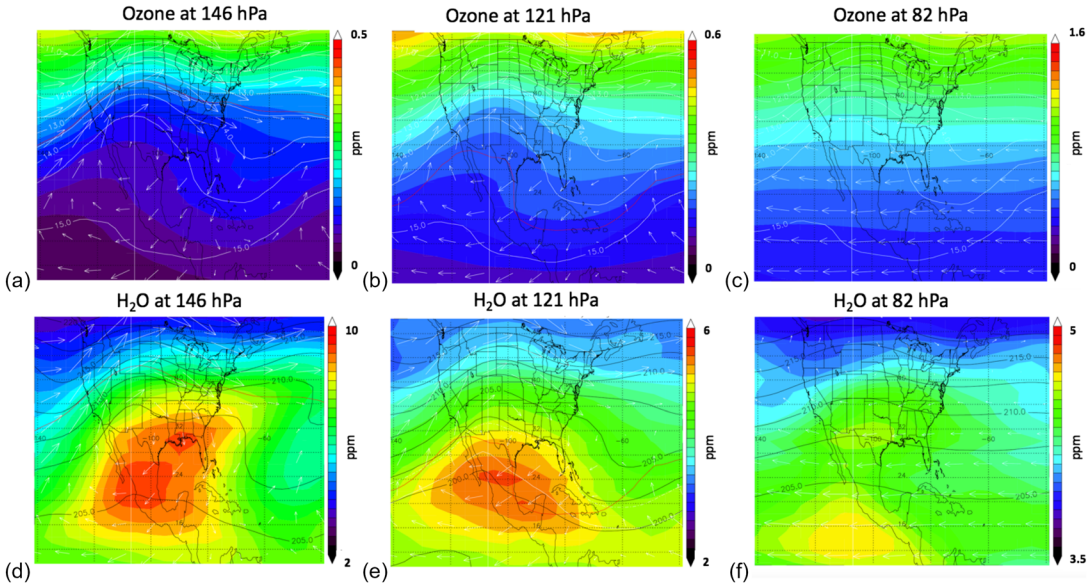

Figure 8. Ozone and water vapor distribution at the two MLS levels below and the one above those shown in Figure 2, (a, d) 146 hPa (~13.4 km), (b, e) 121 hPa (~14.7 km), and (c, f) 82.5 hPa (~17.4 km). For ozone, overlaid contours are tropopause height; for H_2O, the contours are temperature. Wind vectors shown are at the same pressure level. The color bars change for each of the plots.

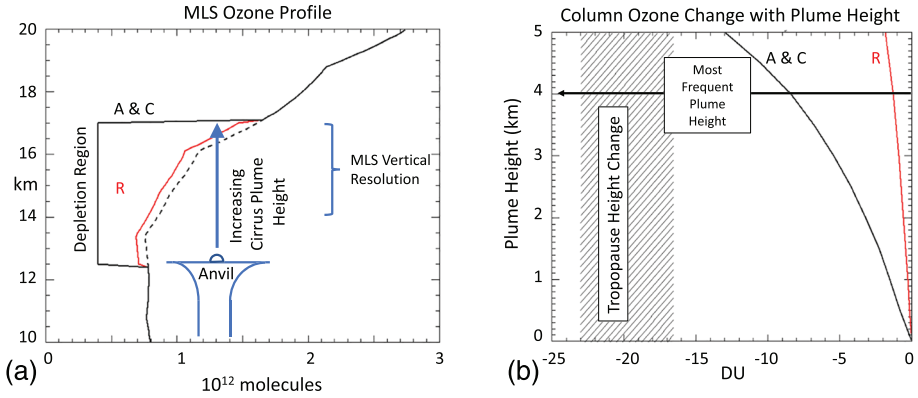

Figure 9. Relative impact of chemical and dynamical ozone column changes. (a) The ozone profile changes for the two cases, the AC high chlorine case and the Robrecht et al. (2019) (R) low chlorine case. Both simulations assume a 20 ppmv enhancement in water. The arrow indicates the range of above-anvil cirrus (plume) height for 12.5–17 km depletion. The approximate vertical resolution of MLS water and ozone measurements is also shown (Livesey et al., 2017). (b) The impact of the ozone loss on the column as a function of the plume height starting with the plume at 12.5 km and moving upward. The hatched area shows the range of column ozone changes due to the monsoonal change in the tropopause height using heights shown in in Figure 6. The horizontal arrow shows the most frequent cirrus plume height above the anvil (Homeyer et al., 2017).

column ozone over the region (see Figure 4b). A 1.5 DU change would be difficult to detect in OMI products and is significantly smaller than the column change produced by monsoon dynamics.

4. Summary and Conclusions

The goal of this study is to look at the impact of the NAM on column ozone and EDD. In part, this study was motivated by the hypothesis put forth by Anderson et al. (2012, 2017) and AC that convective injection of water vapor over the NAM might lead to significant halogenic ozone loss through active chlorine released by heterogeneous reactions on aerosol surfaces. The NAM lowe stratospheric anticyclone could concentrate the chemical ozone loss, and thus produce a noticeable decrease in column ozone. This decrease would be spatially correlated with convectively enhanced high UTLS water vapor, and be associated with increased surface UV exposure (EDD).

The Anderson chemical loss hypothesis controversial (e.g., Homeyer et al., 2014; Schwartz et al., 2013), and if chemical loss occurs it may, quite small. Robrecht et al. (2019), using SEAC^{4}RS data and the CLAMS model simulations showed that ozone losses through heterogeneous chemistry would be <10% percent which would lead to changes in NAM column ozone of at most 1–2 DU.

We have used 10 years (2006–2015) of July–August OMI column ozone and EDD measurements along with MLS trace gas data and ERAi reanalysis data to examine the interrelationship between the trace gas fields over the NAM. By averaging the data over 10 July–August periods, we hoped to isolate any persistent signal of ozone loss against the normal background variability.

The ERAi meteorological fields show that the July–August NAM anticyclonic circulation is centered over northern Mexico/southwest United States in the upper troposphere moving northwestward and weakening with altitude (also see Randel et al., 2015). MLS measurements at 100 hPa show a large water vapor anomaly covering the southern United States and Mexico (Figure 5b) and this anomaly extends from the upper troposphere to the lower stratosphere (Figures 8d–8f). The water vapor anomaly is coincident with NAM elevated convective heights and is likely a result of the evaporation of ice (Dessler & Sherwood, 2004) based on both HDO measurements (Randel et al., 2012) and enhanced water vapor coincident with reduced OLR (Randel et al., 2015).

We find that there is a large correlation between July–August upper troposphere/lower stratosphere (UTLS) water vapor, column ozone decrease, and increased erythemal dosage (Table 1). However, the mechanism behind this relationship is dynamical. It results from monsoonal lifting of the tropopause by 1–2 km compared to tropopause heights at the same latitudes outside the monsoon. This lifting reduces the ozone column by as much as 20 DU producing and increase of 1.2 kJ/m^2 in EDD which is significant. The

monsoon circulation enhances convection and simultaneously lifts the tropopause, reducing the ozone column thereby increasing EDD. The enhanced convection moistens the UTLS creating the water vapor anomaly.

MLS ozone measurements within regions of enhanced water vapor show no apparent anomalous decreases at 100 hPa (Figures 5a and 5c), nor at higher levels (Figure 8). This lack of detectable depletion in lower stratospheric ozone was also noted by Schwartz et al. (2013).

An alternative to the monsoonal convection-driven heterogenous chemical loss mechanism has been suggested by Solomon et al. (2016) for the AM. In their scenario, chlorine reservoir gases at high latitudes are be transported southward by the AM's anticyclonic circulation into the enhanced aerosol region associated with the AM (Vernier et al., 2011, 2015) producing ozone loss. The NAM circulation in the lower stratosphere is weak compared to the AM (as exhibited by the zonal nature of the ozone field shown in Figure 8c and wind vectors), which makes southward meridional transport of HCl and other inorganic chlorine reservoir gases very unlikely. We also note that the coldest temperature zone where possible aerosol activation could occur (Drdla & Müller, 2010) is at the very southern end of the monsoon where the concentration of HCl is observed to be quite low (Froidevaux et al., 2015; Mahieu et al., 2008). Generally, temperatures at higher latitudes and altitudes are too warm for aerosol activation as noted by Schwartz et al. (2013).

Against the background of tropopause lifting and tropopause variability, it will be difficult to detect anomalous chemical ozone loss through changes in the column ozone or EDD. Local decreases in ozone linked to convection may also be the result of low ozone tropospheric air injected into the lower stratosphere (Homeyer et al., 2014). On a longer timescale, it might be possible that net chemical production of ozone is taking place in the upper troposphere, given enhanced NOx production by monsoon lightning, and the vertical transport of VOCs into the region (Pickering et al., 1993). Ozone production and NOx enhancement by convection was not considered in the chemical models simulating ozone loss reported here.

As global warming increases, and monsoon convection intensifies, the NAM may grow in size leading to a more elevated tropopause and higher EDD over a wider region in the southern United States, and there is some evidence that this change is already taking place (Garfin et al., 2013; Luong et al., 2017).

Data Availability Statement

MLS, OMI and ERAi data used in this study are publicly available from NASA and the European Center for Medium Range Forecasting at no charge. Satellite convective height data are described in Ueyama et al. (2018) and Schoeberl et al. (2019) as well as this paper; the data set is unrestricted, available at no cost, and can be downloaded from https://bocachica.arc.nasa.gov/nasaarc_cldalt/. Documentation of the data set including methodology and file structure are also on this server. Please contact leonhard.pfister@nasa.gov for questions. Level 3 NEXRAD data are available from: http://doi.org/10.5065/D6NK3CR7. This work was supported under NASA grant 80NSSC19K0757.

Acknowledgments
The authors would like to thank the reviewers for very insightful and helpful comments.

References

Adams, D., & Comrie, A. (1997). The North American monsoon. *Bulletin of the American Meteorological Society*, *78*(10), 2197–2213. https://doi.org/10.1175/1520-0477(1997)078<2197:TNAM>2.0.CO;2

Anderson, J. G., & Clapp, C. E. (2018). Coupling free radical catalysis, climate change, and human health. *Physical Chemistry Chemical Physics*, *20*, 10,569–10,587. https://doi.org/10.1039/C7CP08331A

Anderson, J. G., Weisenstein, D. K., Bowman, K. P., Homeyer, C. R., Smith, J. B., Wilmouth, D. M., et al. (2017). Stratospheric ozone over the United States in summer linked to observations of convection and temperature via chlorine and bromine catalysis. *PNAS*, *114*(25), E4905–E4913. https://doi.org/10.1073/pnas.1619318114

Anderson, J. G., Wilmouth, D. M., Smith, J. B., & Sayres, D. S. (2012). UV dosage levels in summer: Increased risk of ozone loss from convectively injected water vapor. *Science*, *337*(6096), 835–839. https://doi.org/10.1126/science.1222978

Arola, A., Kazadzis, S., Lindfors, A., Krotkov, N., Kujanpää, J., Tamminen, J., et al. (2009). A new approach to correct for absorbing aerosols in OMI UV. *Geophysical Research Letters*, *36*, L22805. https://doi.org/10.1029/2009GL041137

Bergman, J. W., Fierli, F., Jensen, E. J., Honomichl, S., & Pan, L. L. (2013). Boundary layer sources for the Asian anticyclone: Regional contributions to a vertical conduit. *Journal of Geophysical Research: Atmospheres*, *118*, 2560–2575. https://doi.org/10.1002/jgrd.50142

Brasseur, G., & Solomon, S. (2016). *'Aeronomy of the middle atmosphere', Atmospheric and Oceanographic Sciences Library* (Vol. 25, p. 646). Netherlands: Springer. https://doi.org/10.1007/1-4020-3824-0

Clapp, C. E., Smith, J. B., Bedka, K. M., & Anderson, J. G. (2019). Identifying source regions and the distribution of cross-tropopause convective outflow over North America during the warm season. *Journal of Geophysical Research: Atmospheres*, *124*, 13,750–13,762. https://doi.org/10.1029/2019JD031382

Cooney, J. W., Bowman, K. P., Homeyer, C. R., & Fenske, T. M. (2018). Ten year analysis of tropopause-overshooting convection using GridRad data. *Journal of Geophysical Research: Atmospheres*, *123*, 329–343. https://doi.org/10.1002/2017JD027718

Dee, D. P., Uppala, S. M., Simmons, A. J., Berrisford, P., Poli, P., Kobayashi, S., et al. (2011). The ERA-Interim reanalysis: Configuration and performance of data assimilation system. *Quarterly Journal of the Royal Meteorological Society*, *137*(656), 553–597. https://doi.org/10.1002/qj.828

Dessler, A. E., & Sherwood, S. C. (2004). Effect of convection on the summertime extratropical lower stratosphere. *Journal of Geophysical Research*, *109*, D23301. https://doi.org/10.1029/2004JD005209

Drdla, K., & Müller, R. (2010). Temperature thresholds for polar stratospheric ozone loss. *Atmospheric Chemistry and Physics Discussions*, *10*, 28,687–28,720. https://doi.org/10.5194/acpd-10-28687-2010

Froidevaux, L., Anderson, J., Wang, H.-J., Fuller, R. A., Schwartz, M. J., Santee, M. L., et al. (2015). Global OZone Chemistry and Related trace gas Data records for the Stratosphere (GOZCARDS): Methodology and sample results with a focus on HCl, H_2O, and O_3. *Atmospheric Chemistry and Physics*, *15*(18), 10,471–10,507. https://doi.org/10.5194/acp-15-10471-2015

Garfin, G., Jardine, A., Merideth, R., Black, M., & Leroy, S. (Eds.) (2013). *Assessment of climate change in the southwest United States: A report prepared for the National Climate Change Assessment* (p. 531). Washington, DC: Island Press. https://doi.org/10.5822/978-1-61091-484-0

Hanisco, T., Moyer, E. J., Weinstock, E. M., St. Clair, J. M., Sayres, D. S., Smith, J. B., et al. (2006). Observations of deep convective influence on stratospheric water vapor and its isotopic composition. *Geophysical Research Letters*, *34*, L04814. https://doi.org/10.1029/2006GL027899

Herman, R. L., Ray, E. A., Rosenlof, K. H., Bedka, K. M., Schwartz, M. J., Read, W. G., et al. (2017). Enhanced stratospheric water vapor over the summertime continental United States and the role of overshooting convection. *Atmospheric Chemistry and Physics*, *17*, 6113–6124. https://doi.org/10.5194/acp-17-6113-2017

Homeyer, C. R. (2014). Formation of the enhanced-V infrared cloud-top feature from high-resolution three-dimensional radar observations. *Journal of the Atmospheric Sciences*, *71*, 332–348. https://doi.org/10.1175/JAS-D-13-079.1

Homeyer, C. R., McAuliffe, J. D., & Bedka, K. M. (2017). On the development of above-anvil cirrus plumes in extratropical convection. *Journal of the Atmospheric Sciences*, *74*, 1617–1633. https://doi.org/10.1175/JAS-D-16-0269.1

Homeyer, C. R., Pan, L. L., Dorsi, S. W., Avallone, L. M., Weinheimer, A. J., O'Brien, A. S., et al. (2014). Convective transport of water vapor into the lower stratosphere observed during double tropopause events. *Journal of Geophysical Research: Atmospheres*, *119*, 10,941–10,958. https://doi.org/10.1002/2014JD021485

Huffman, G. J., Adler, R. F., Bolvin, D. T., Gu, G., Nelkin, E. J., Bowman, K. P., et al. (2007). The TRMM multi-satellite precipitation analysis: Quasi-global, multi-year, combined-sensor precipitation estimates at fine scale. *Journal of Hydrometeorology*, *8*(1), 38–55.

Levelt, P., van den Oord, G. H. J., Dobber, M. R., Malkki, A., Visser, H., de Vries, J., et al. (2006). The ozone monitoring instrument. *IEEE Transactions on Geoscience and Remote Sensing*, *44*(5), 1093–1101. https://doi.org/10.1109/TGRS.2006.872333

Livesey, N., Read, W. G., Wagner, P. A., Froidevaux, L., Lambert, A., Manney, G. L., et al. (2017). *Aura Microwave Limb Sounder (MLS) Version 4.2x Level 2 data quality and description document, JPL D-33509 Rev. C*.

Luong, T., Castro, C., Chang, H.-I., Lahmers, T., Adams, D., & Ochoa-Moya, C. (2017). The more extreme nature of the North American monsoon precipitation in the southwestern United States as revealed by historical climatology of simulated severe weather events. *Journal of Applied Meteorology and Climatology*, *56*(2), 2509–2529. https://doi.org/10.1175/JAMC-D-16-0358.1

Mahieu, E., Duchatelet, P., Demoulin, P., Walker, K. A., Dupuy, E., Froidevaux, L., et al. (2008). Validation of ACE-FTS v2.2 measurements of HCl, HF, CCl_3F and CCl_2F_2 using space-, balloon- and ground-based instrument observations. *Atmospheric Chemistry and Physics*, *8*, 6199–6221. https://doi.org/10.5194/acp-8-6199-2008

Minnis, P., Yost, C. R., Sun-Mack, S., & Chen, Y. (2008). Estimating the top altitude of optically thick ice clouds from thermal infrared satellite observations using CALIPSO data. *Geophysical Research Letters*, *35*, L12801. https://doi.org/10.1029/2008GL033947

Pan, L. L., Honomichl, S. B., Kinnison, D. E., Abalos, M., Randel, W. J., Bergman, J. W., & Bian, J. (2016). Transport of chemical tracers from the boundary layer to stratosphere associated with the dynamics of the Asian summer monsoon. *Journal of Geophysical Research: Atmospheres*, *121*, 14,159–14,174. https://doi.org/10.1002/2016JD025616

Park, M., Randel, W. J., Gettelman, A., Massie, S. T., & Jiang, J. H. (2007). Transport above the Asian summer monsoon anticyclone inferred from Aura Microwave Limb Sounder tracers. *Journal of Geophysical Research*, *112*, D16309. https://doi.org/10.1029/2006JD008294

Pickering, K. E., Thompson, A., Tao, W.-K., & Kucsera, T. (1993). Upper tropospheric ozone production following mesoscale convection during STEP/EMEX. *Journal of Geophysical Research*, *98*. https://doi.org/10.1029/93JD00875

Qu, Z., Huang, Y., Vaillancourt, P. A., Cole, J. N. S., Milbrandt, J. A., Yau, M.-K., et al. (2020). Simulation of convective moistening of the extratropical lower stratosphere using a numerical weather prediction model. *Atmospheric Chemistry and Physics*, *20*, 2143–2159. https://doi.org/10.5194/acp-20-2143-2020

Randel, W. J., Moyer, E., Park, M., Jensen, E., Bernath, P., Walker, K., & Boone, C. (2012). Global variations of HDO and HDO/H_2O ratios in the upper troposphere and lower stratosphere derived from ACE-FTS satellite measurements. *Journal of Geophysical Research*, *117*, D06303. https://doi.org/10.1029/2011JD016632

Randel, W. J., Zhang, K., & Fu, R. (2015). What controls stratospheric water vapor in the NH summer monsoon regions? *Journal of Geophysical Research: Atmospheres*, *120*, 7988–8001. https://doi.org/10.1002/2015JD023622

Robrecht, S., Vogel, B., Grooß, J.-U., Rosenlof, K., Thornberry, T., Rollins, A., et al. (2019). Mechanism of ozone loss under enhanced water vapour conditions in the mid-latitude lower stratosphere in summer. *Atmospheric Chemistry and Physics*, *19*, 5805–5833.

Santee, M. L., Manney, G. L., Livesey, N. J., Schwartz, M. J., Neu, J. L., & Read, W. G. (2017). A comprehensive overview of the climatological composition of the Asian summer monsoon anticyclone based on 10 years of Aura Microwave Limb Sounder measurements. *Journal of Geophysical Research: Atmospheres*, *122*, 5491–5514. https://doi.org/10.1002/2016JD026408

Sassen, K., & Wang, Z. (2008). Classifying clouds around the globe with the CloudSat Radar: 1 year of results. *Geophysical Research Letters*, *35*, L04805. https://doi.org/10.1029/2007GL032591

Schoeberl, M. R., Jensen, E. J., Pfister, L., Ueyama, R., Wang, T., Selkirk, H., et al. (2019). Water vapor, clouds, and saturation in the tropical tropopause layer. *Journal of Geophysical Research: Atmospheres*, *124*, 3984–4003. https://doi.org/10.1029/2018JD029849

Schwartz, M. J., Read, W. J., Santee, M. L., Livesey, N. J., Froidevaux, L., Lambert, A., & Manney, G. L. (2013). Convectively injected water vapor in the North American summer lowermost stratosphere. *Geophysical Research Letters*, *40*, 2316–2321. https://doi.org/10.1002/grl.50421

Sherwood, S. C., Chae, J.-H., Minnis, P., & McGill, M. (2004). Underestimation of deep convective cloud tops by thermal imagery. *Geophysical Research Letters*, *31*, L11102. https://doi.org/10.1029/2004GL019699

Shi, Q., Jayne, J., Kolb, C., Worsnop, D., & Davidovits, P. (2001). Kinetic model for the reaction of $ClONO_2$ with H_2O and HCl and HOCl with HCl in sulfuric acid solutions. *Journal of Geophysical Research*, *106*, 24,259–24,274.

Smith, J. B., Wilmouth, D. M., Bedka, K. M., Bowman, K. P., Homeyer, C. R., Dykema, J. A., et al. (2017). A case study of convectively sourced water vapor observed in the overworld stratosphere over the United States. *Journal of Geophysical Research: Atmospheres*, *122*, 9529–9554. https://doi.org/10.1002/2017JD026831

Solomon, S., Kinnison, D., Garcia, R. R., Bandoro, J., Mills, M., Wilka, C., et al. (2016). Monsoon circulations and tropical heterogeneous chlorine chemistry in the stratosphere. *Geophysical Research Letters*, *43*, 12,624–12,633. https://doi.org/10.1002/2016GL071778

Staehelin, J., Harris, N., Appenzeller, C., & Eberhard, J. (2001). Ozone trends: A review. *Reviews of Geophysics*, *39*, 231–290.

Steinbrecht, W., Claude, H., Kohler, U., & Hoinka, K. P. (1998). Correlations between tropopause height and total ozone: Implications for long-term changes. *Journal of Geophysical Research*, *103*, 19,183–19,192.

Tanskanen, A., Lindfors, A., Määttä, A., Krotkov, N., Herman, J., Kaurola, J., et al. (2007). Validation of daily erythemal doses from Ozone Monitoring Instrument with ground-based UV measurement data. *Journal of Geophysical Research*, *112*, D24S44. https://doi.org/10.1029/2007JD008830

Thornton, B. F., Toohey, D. W., Tuck, A. F., Elkins, J. W., Kelly, K. K., Hovde, S. J., et al. (2007). Chlorine activation near the midlatitude tropopause. *Journal of Geophysical Research*, *112*, D18306. https://doi.org/10.1029/2006JD007640

Ueyama, R., Jensen, E., Pfister, L., Diskin, G., Bui, P., & Dean-Day, J. (2014). Dehydration in the tropical tropopause layer: A case study for model evaluation using aircraft observations. *Journal of Geophysical Research: Atmospheres*, *119*, 5299–5316. https://doi.org/10.1002/2013JD021381

Ueyama, R., Jensen, E. J., & Pfister, L. (2018). Convective influence on the humidity and clouds in the tropical tropopause layer during boreal summer. *Journal of Geophysical Research: Atmospheres*, *123*, 7576–7593. https://doi.org/10.1029/2018JD028674

Vernier, J.-P., Fairlie, T. D., Natarajan, M., Wienhold, F. G., Bian, J., Martinsson, B. G., et al. (2015). Increase in upper tropospheric and lower stratospheric aerosol levels and its potential connection with Asian pollution. *Journal of Geophysical Research: Atmospheres*, *120*, 1608–1619. https://doi.org/10.1002/2014JD022372

Vernier, J.-P., Thomason, L. W., & Kar, J. (2011). CALIPSO detection of an Asian tropopause aerosol layer. *Geophysical Research Letters*, *38*, L07804. https://doi.org/10.1029/2010GL046614

Wang, X., Dessler, A. E., Schoeberl, M. R., Yu, W., & Wang, T. (2019). Impact of convectively lofted ice on the seasonal cycle of water vapor in the tropical tropopause layer. *Atmospheric Chemistry and Physics*, *19*, 14,621–14,636. https://doi.org/10.5194/acp-19-14621-2019

WHO (2006). *Solar ultraviolet radiation—Global burden of disease from solar ultraviolet radiation*, *Environmental Burden of Disease Series*, ISBN 92-4159440-3 (Vol. 13). Geneva, Switzerland: World Health Organization.

Zhang, H., Wang, J., Garcia, L., Zeng, J., Dennhardt, C., Lon, Y., & Krotkov, N. (2019). Surface erythemal UV irradiance in the continental United States derived from ground-based and OMI observations: Quality assessment, trend analysis and sampling issues. *Atmospheric Chemistry and Physics*, *19*, 2165–2281.

Zhisheng, A., Guoxiong, W., Jianping, L., Youbin, S., Yimin, L., Weijian, Z., et al. (2015). Global monsoon dynamics. *Annual Review of Earth and Planetary Sciences*, *43*(1), 29–77. https://doi.org/10.1146/annurev-earth-060313-054623

Zhou, Y., Meng, X., Belle, J., Zhang, H., Kennedy, C., Al-Hamdan, M., et al. (2019). Compilation and spatio-temporal analysis of publicly available total solar and UV irradiance data in the contiguous United States. *Environmental Pollution*, *253*, 130–140.